



OPEN Projecting XRP price burst by correlation tensor spectra of transaction networks

Abhijit Chakraborty^{1,2✉}, Tetsuo Hatsuda² & Yuichi Ikeda¹

Cryptoassets are becoming essential in the digital economy era. XRP is one of the large market cap cryptoassets. Here, we develop a novel method of correlation tensor spectra for the dynamical XRP networks, which can provide an early indication for XRP price. A weighed directed weekly transaction network among XRP wallets is constructed by aggregating all transactions for a week. A vector for each node is then obtained by embedding the weekly network in continuous vector space. From a set of weekly snapshots of node vectors, we construct a correlation tensor. A double singular value decomposition of the correlation tensors gives its singular values. The significance of the singular values is shown by comparing with its randomize counterpart. The evolution of singular values shows a distinctive behavior. The largest singular value shows a significant negative correlation with XRP/USD price. We observe the minimum of the largest singular values at the XRP/USD price peak during the first week of January 2018. The minimum of the largest singular value during January 2018 is explained by decomposing the correlation tensor in the signal and noise components and also by evolution of community structure.

Cryptoassets represent value that one can transfer, store, or trade digitally. It uses cryptography to protect data and distributed ledger technology to record transactions. A blockchain technology, which is a form of secure digital ledger, is used to store the records of crypto transactions. Recently, cryptoassets have been very popular as an investment, but cryptoasset prices are extremely volatile and unpredictable. The cryptomarket experienced severe price fluctuations from 2017, December to 2018, January. The presence of bubbles i.e., explosive price behavior in this asset has attracted attention from the researchers. At present, there are many cryptoassets. Some well-known of them are Bitcoin (BTC), Ethereum (ETH) and XRP. For the last one decade complex network theory has been widely used to analyze cryptoasset transaction data. Among the cryptoassets, networks of BTC and ETH transactions have been studied extensively¹, which include different structural properties^{2,3}, temporal evolution^{2,4-6} and market effect⁷⁻⁹ of these networks. In contrast, XRP transactions have been less explored. Ripple Labs Inc. created XRP as the native cryptocurrency for the Ripple network, which is designed to provide fast, efficient, and cost-effective financial transactions. The Ripple network is used for real-time gross settlement of financial transactions, currency exchange, and cross-border remittances. The goal of the Ripple network is to provide a stable and decentralized ledger system that can be used to facilitate cross-border transactions in a more efficient and cost-effective manner. XRP is used as a bridge currency in the network, helping to facilitate cross-border transfers and providing liquidity to the system. Moreno-Sanchez et al. uncovered community formation and clustering properties for the Ripple network¹⁰. Y. Ikeda studied the structural properties of XRP transaction network, which include the heavy tail nature of nodal strength distributions, low value of clustering coefficient and significant triangular motif¹¹. More recently, the role of the most active nodes with respect to outgoing and incoming flows for a duration including bubble/crash period has been quantified for BTC and XRP transaction networks¹².

Any statistical dependence between a pair of variables can be studied by cross correlation which is predictive and useful for empirical data. It can be measured in different ways: One of the simple and well-known methods is the Pearson correlation which represents the linear dependence between variables and is defined for a pair of variables x and y with n observations as $\rho = \sum_{i=1}^n (x_i - \bar{x})(y_i - \bar{y}) / ((n-1)\sigma_x\sigma_y)$. Here \bar{x} , \bar{y} , and σ_x , σ_y indicate mean and standard deviations of x and y . The cross correlation methodology armed with random matrix theory (RMT) is mostly applied to time series data. The aim of such method is to analyze high dimensional data to find key factors for the collective dynamics of many quantities. For example, it is used to study the daily returns of

¹Graduate School of Advanced Integrated Studies in Human Survivability, Kyoto University, Kyoto 606-8306, Japan. ²RIKEN Interdisciplinary Theoretical and Mathematical Sciences Program, Saitama 351-0198, Japan. ✉email: chakraborty.abhijit.7y@kyoto-u.ac.jp

different stocks^{13–15} and foreign exchange rates^{16,17}, monthly macroeconomic data¹⁸, or different medical data such as electroencephalogram, magnetoencephalography data recording¹⁹. Also, Kondor et al. applied principal component analysis on the matrices obtained from the daily network snapshots to show the relationship between the price of bitcoin with structural changes in the transaction network²⁰. The application of cross correlation on stock market data shows the relationship between stock price changes and liquidity or trading volume²¹. Note that these are time series of variables that emerge due to interactions of different entities of the system. In most cases, we lack detail information of the interactions at the micro level. For example, we do not have detail information about the interaction among the individuals in stock markets.

In the case of XRP, we know the information for all transactions between wallets. Using this high-quality micro level data, we develop a method of cross correlation tensor which can be applied on dynamical XRP transaction networks. Our method relates the structural properties of XRP networks to the XRP/USD price. To calculate the correlation tensor, nodes of the networks are converted to vectors using network embedding techniques^{22,23}. We use the DeepWalk embedding technique²², which uses a set of truncated random walks to learn latent features. The latent features capture neighborhood information and community memberships of the nodes. Using a network as the input, the algorithm provides a latent representation in a continuous vector space as an output. A generalization of the DeepWalk algorithm is node2vec²³, which uses biased random walks to learn features that encode more complex relations of nodes, such as functional relationships. Using the vector representation for a subset of nodes present in every weekly XRP transaction networks, we calculate correlation tensors for different time periods. We perform a double singular value decomposition on the correlation tensors to obtain its spectra. We compare the results with reference correlation tensors to understand the significance. As a reference correlation tensor, one usually uses the RMT method. However, as we are using a small time window to calculate the correlation tensor, RMT method will not be suitable as reference. We use randomized and reshuffled correlation tensors as reference correlation tensors. The largest few singular values capture the impact of the bubble period or crash in XRP price. The largest singular value is found to be significant and has a strong negative correlation with XRP/USD price. Furthermore, it provides an early indication for XRP/USD price, including bubble periods or crashes.

Results

The weekly network obtained from XRP transactions between wallets evolves with time. We focus our study on the duration 2017 October 02 to 2018 March for which covers a bubble period in XRP price. It indicates 22 weekly networks. The number of nodes for each weekly network is shown in Fig. 1a. We observe that the number of nodes of the weekly networks increases rapidly from 45, 169 during the week of 2017, November 27–December 04 to the peak value 209, 143 during the week of 2018, January 01–January 07 and later further falls to 27, 811 during the week of 2018, February 26 to March 04. Figure 1b shows the decline in the number of links per node indicating the average nodal in- or out-degree from 2.15 to 1.20 during 2017, October 02–2018 March 04. The decline in the number of links per node indicates a reduction in the average frequency of transactions of a node with other distinct nodes. We note that XRP transaction volume was very high for three weeks between December 05–December 24 and also for the week during 2018, January 22–January 29, as shown in Fig. 1c. The three weeks of extremely high XRP transaction volume may have contributed to the bubble formation in XRP/USD during 2017, December 25 to 2018 January 07. The daily XRP/USD price from October 2, 2017 to March 4, 2018 is shown in Fig. 1d. The XRP/USD price had an extraordinary rise and fall between December 2017 and January 2018. This indicates a bubble period for XRP. We consider this period for our study because this is the most significant bubble period for the cryptoasset market. The chart of XRP/USD prices for a more extended period is shown in SI Fig. S1.

We have embedded each of these weekly networks using the well-known DeepWalk algorithm on $D = 32$ -dimensional space. For the details of the embedding technique, see “Data and methods” section. This gives a D -dimensional vector V_i^α for each node of the networks. We use i, j as node indices and Greek letters α, β as components of the vectors on a D dimensional space. In weekly networks of XRP transactions, we found $N = 71$ nodes does at least one transaction every week. We call these $N = 71$ nodes, regular nodes. Each regular node of weekly networks in the embedding space is represented by a D -dimensional vector time series $V_i^\alpha(t)$, where $i = 1, 2, 3, \dots, N, t = 1, 2, 3, \dots, T$ and $\alpha = 1, 2, 3, \dots, D$. We have chosen $D = 32$ for our study. Other values of D give qualitatively similar results. Later, we provide the quantitative dependence on D in Eq. (11).

The correlation tensor between the different components of the regular nodes is defined as

$$M_{ij}^{\alpha\beta}(t) = \frac{1}{2\Delta T} \sum_{t'=t-\Delta T}^{t+\Delta T} \frac{[V_i^\alpha(t') - \overline{V}_i^\alpha][V_j^\beta(t') - \overline{V}_j^\beta]}{\sigma_{V_i^\alpha} \sigma_{V_j^\beta}}, \quad (1)$$

where \sum is taken over 5 weekly $\{t-2, t-1, t, t+1, t+2\}$ networks with $\Delta T = 2$ for our analysis. The \overline{V}_i^α and $\sigma_{V_i^\alpha}$ represents mean and standard deviation of V_i^α over a time window of $(2\Delta T + 1) = 5$ weekly $\{t-2, t-1, t, t+1, t+2\}$ networks. Note that lower the values of ΔT , more noise is present in the obtained correlation tensor. We also can not take ΔT too large as we are studying the dynamical evolution of the networks. We further discuss the dependence of the correlation tensor on the time window in the SI Text 2.

To understand the significance of the empirical correlation tensor, we consider the following two null hypotheses. The null hypothesis of the components of embedding vectors for regular nodes, V_i^α (randomize), are independent, uniformly distributed, random variables within $[-1, 1]$. We obtained the randomized correlation tensor from V_i^α (randomize). Another method to randomize the empirical correlation tensor is to remove the correlation present between the different components of the embedding vectors, by reshuffling the positions of the components of embedding vectors V_i^α (reshuffle). We obtain the reshuffle correlation tensor from V_i^α (reshuffle). The

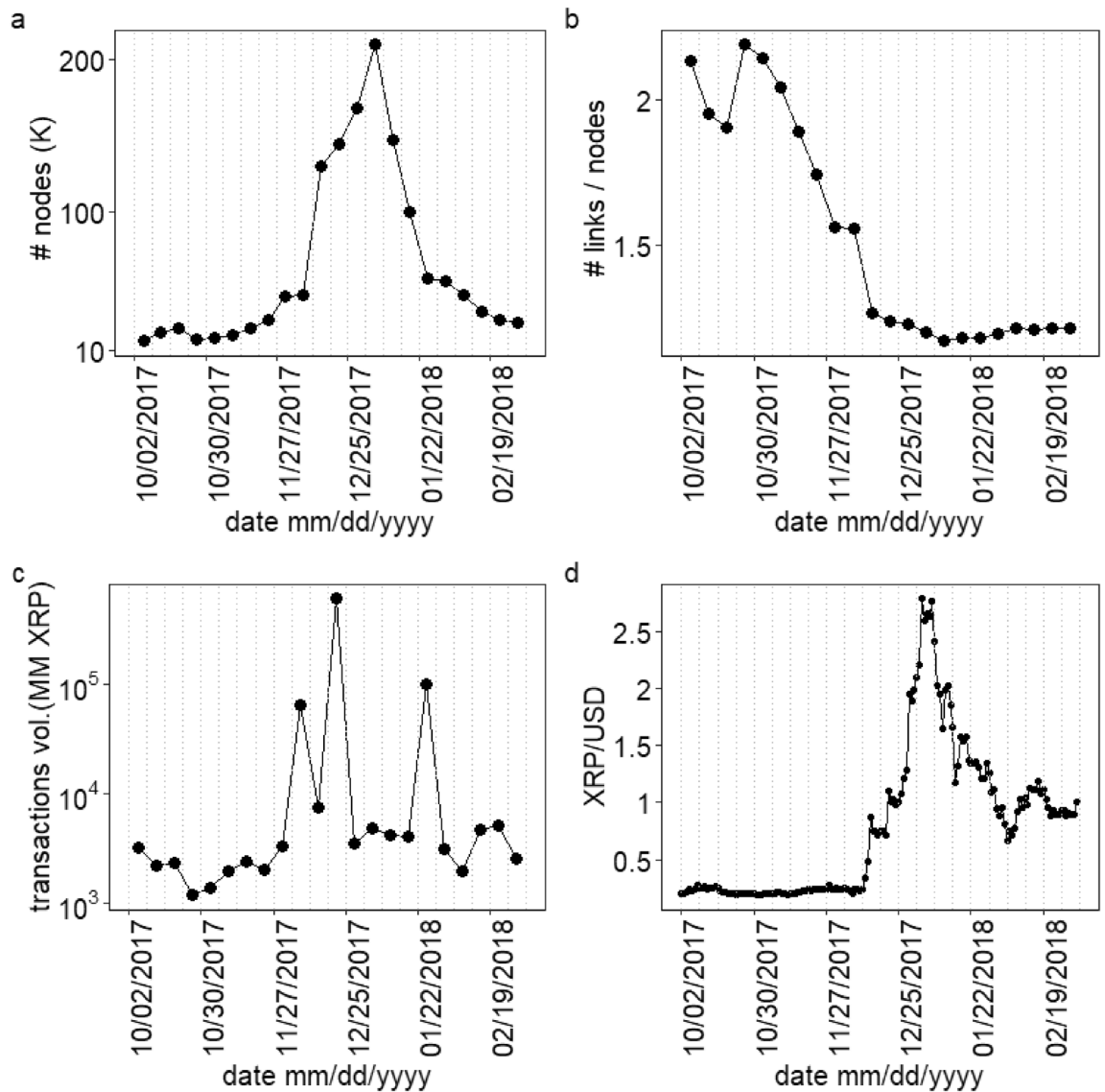


Figure 1. The variation of (a) total number of nodes (b) number of links per node and (c) total transaction volume in millions XRP for each weekly network. (d) The daily XRP/USD close price (source: <https://www.marketwatch.com/investing/cryptocurrency/xrpUSD>). The dotted grey vertical lines represent the weekly windows.

distributions of the elements of empirical, randomize and reshuffle correlation tensor are shown in Fig. 2 for the week of 2017, November 06–November 12. We have taken the average of the data for the distributions with 20 different runs of the embedding algorithm. The distributions from randomized and reshuffled correlation tensors are qualitatively identical. This is because the auto correlation for different components of the empirical embedding vectors vanishes when the lag is more than one week. These two distributions are symmetrical around zero, with an average value of the elements close to zero. The empirical correlation differs from the randomized and reshuffle correlation tensor. It is an asymmetric distribution having an average value of the elements 0.017. The correlation tensor has the dimension $N \times N \times D \times D$. Since we have many elements in the correlation tensor, we uncover the crucial information by diagonalizing it using a double singular value decomposition (SVD) method. The double SVD is a natural extension of the single SVD for the correlation of standard non-embedded vectors V_i . Since indices i and α correspond to the individual node and the embedding dimension, respectively, it is also natural to carry out SVD successively with the (i, j) -pair and with the (α, β) -pair separately as discussed in the “Data and methods” section.

A double SVD of the correlation tensor gives us $N \times D$ singular values ρ_k^γ , where $i = 1, 2, 3, \dots, N$ and $\gamma = 1, 2, 3, \dots, D$. For the details, refer to the “Data and methods” section. We compare the singular values ρ_k^γ of the empirical correlation tensor with the singular values of randomized correlation tensor ρ_k^γ (randomize) and reshuffled correlation tensor ρ_k^γ (reshuffle). The comparison is shown in Fig. 3 for the week of 2017, November 06–November 12. This shows that the largest singular value lies beyond the largest singular value of the

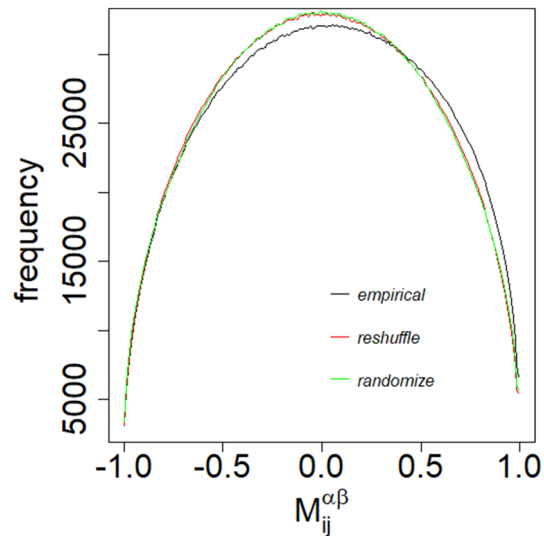


Figure 2. The distributions of the elements of empirical, reshuffle and randomize correlation tensors calculated for the week, November 06 to November 12, 2017. The data are averaged over 20 uncorrelated embedding of the networks.

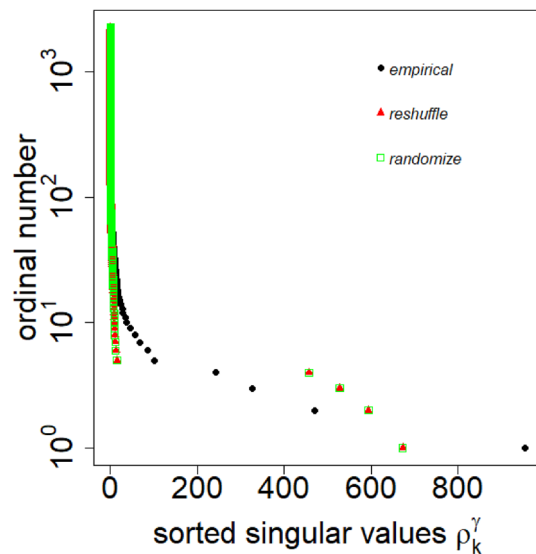


Figure 3. Sorted singular values ρ_k^γ of the empirical, reshuffle and randomize correlation tensor for the week, November 06 to November 12, 2017. The values represent average over 20 uncorrelated embeddings of the network.

randomized correlation tensor. Also, the spectral gap ($\rho_1^1 - \rho_2^1$) in the empirical correlation tensor is significantly large compared with its random counterpart.

The temporal variation of the largest singular values of empirical $\rho_k^\gamma(t)$ and reshuffle $\tilde{\rho}_k^\gamma(t)$ correlation tensor for different weeks is shown in Fig. 4. It is evident that the largest singular value ρ_1^1 is well above the largest singular values $\tilde{\rho}_1^1$ of the randomized correlation tensor for all weeks. However, the second largest singular value ρ_2^1 lies below the randomized counterpart. Similar to the largest singular value ρ_1^1 , the spectral gap ($\rho_1^1 - \rho_2^1$) appears significantly higher than that of the randomized case. Moreover, we observe $\tilde{\rho}_k^\gamma(t)$ remains approximately constant with time. In a stark contrast, the largest two empirical singular values and as well as a few more singular values (not shown) vary distinctively for different weeks. Note that normalizing the spectral gaps by their maximum value would make the spectral gaps of the empirical and randomized data comparable in scale, but it would not adequately demonstrate the difference in their magnitudes.

To investigate the relationship between singular values ρ_k^γ and XRP/USD price, we compare the variation of XRP/USD daily price with the largest singular value ρ_1^1 , the second largest singular value ρ_2^1 and the spectral

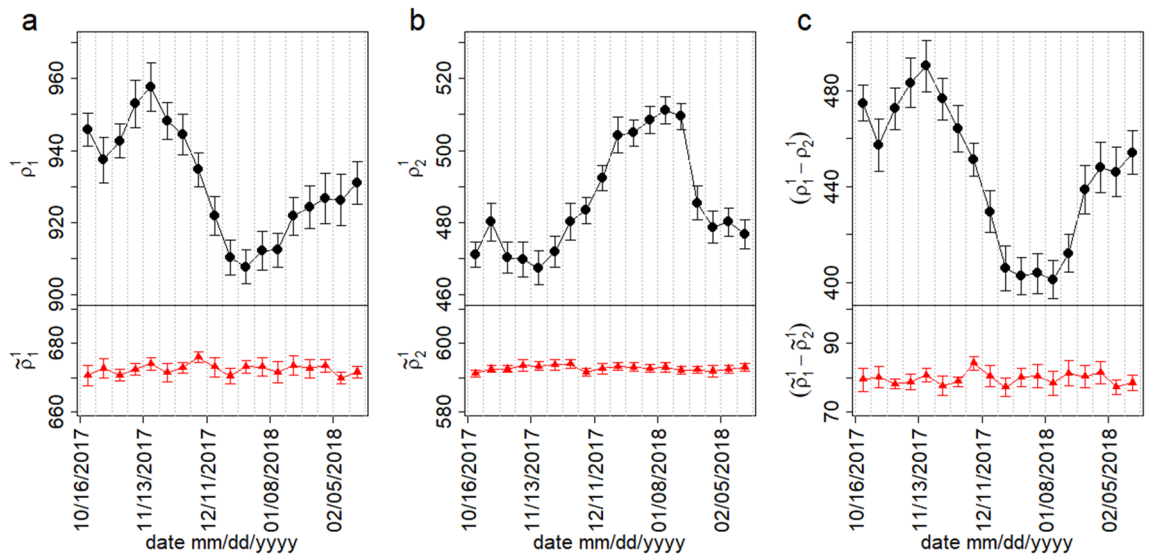


Figure 4. Evolution of the singular values for empirical ρ_k^γ and reshuffled $\tilde{\rho}_k^\gamma$ correlation tensors for different weeks. **(a)** Variation of the largest singular value for empirical ρ_1^1 and reshuffled $\tilde{\rho}_1^1$ correlation tensors. **(b)** Variation of the second largest singular value for empirical ρ_2^1 , reshuffled $\tilde{\rho}_2^1$ correlation tensors. **(c)** Variation of spectral gap for empirical $(\rho_1^1 - \rho_2^1)$ and reshuffled $(\tilde{\rho}_1^1 - \tilde{\rho}_2^1)$ correlation tensors. The error bars indicate the standard deviation. The data are averaged over 20 uncorrelated embeddings of the networks. The dotted grey vertical lines represent the weekly windows.

gap $(\rho_1^1 - \rho_2^1)$ in Fig. 5a–c. To quantify the dependence, we measure the correlation between the weekly XRP/USD price and the two largest singular values ρ_1^1, ρ_2^1 respectively. The weekly XRP/USD price indicates the average daily closing price of XRP/USD for the week. Let us denote the weekly XRP/USD price as $\overline{\text{XRP/USD}}$. The Pearson correlation between $\rho_1^1(t)$ and $\overline{\text{XRP/USD}}(t + 1)$ is found $r = -0.908$ and $p\text{-value} = 1.912 \times 10^{-7}$. The Pearson correlation between ρ_2^1 and $\overline{\text{XRP/USD}}(t + 1)$ is found $r = 0.847$ and $p\text{-value} = 9.22 \times 10^{-6}$. Furthermore, we perform a multi-linear regression of $\overline{\text{XRP/USD}}(t + 1) \sim C_0 + C_1\rho_1^1(t) + C_2\rho_2^1(t)$, gives $C_0 = 27.91, C_1 = -0.033, C_2 = 0.008$ and only the variable $\rho_1^1(t)$ is significant. We found $R^2 = 0.8091$ and $p\text{-value} = 1.581 \times 10^{-6}$, indicating that the 80% variation of $\overline{\text{XRP/USD}}(t + 1)$ can be explained by the largest singular value $\rho_1^1(t)$. We also observe there are significant correlation between singular values and weekly XRP/USD price with two weeks lead $\overline{\text{XRP/USD}}(t + 2)$ and three weeks lead $\overline{\text{XRP/USD}}(t + 3)$, which is described in detail in SI Text 3. Correlation between $\overline{\text{XRP/USD}}(t + 3)$ and $\rho_1^1(t)$ is found to be $r = -0.68$ and $p\text{-value} = 0.001$. This indicates that the largest singular value ρ_1^1 can give an early signal for XRP/USD price.

We also observe that the minimum of $\rho_1^1(t)$ appears during the week of 2017 December 25–December 31. The decomposition of the correlation tensor $M_{ij}^{\alpha\beta}$ into signal $M_{ij}^{\alpha\beta}(\text{signal})$ and noise component $M_{ij}^{\alpha\beta}(\text{noise})$ can explain the reason for this minima. The decomposition of correlation tensor $M_{ij}^{\alpha\beta}$ for the week of 2017, November 06–November 12 is shown in Fig. 6a, which indicates that the distribution of the elements of the signal

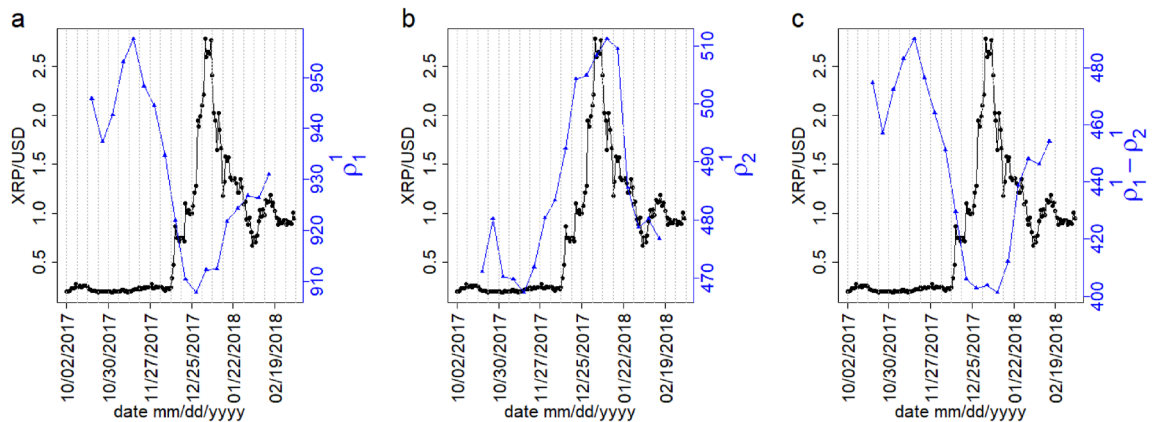


Figure 5. The comparison of daily XRP/USD price (black curves) with **(a)** the largest singular value ρ_1^1 , **(b)** the second largest singular value ρ_2^1 and **(c)** the spectral gap $(\rho_1^1 - \rho_2^1)$ of correlation tensors for different weeks (blue curves). The dotted grey vertical lines represent the weekly windows.

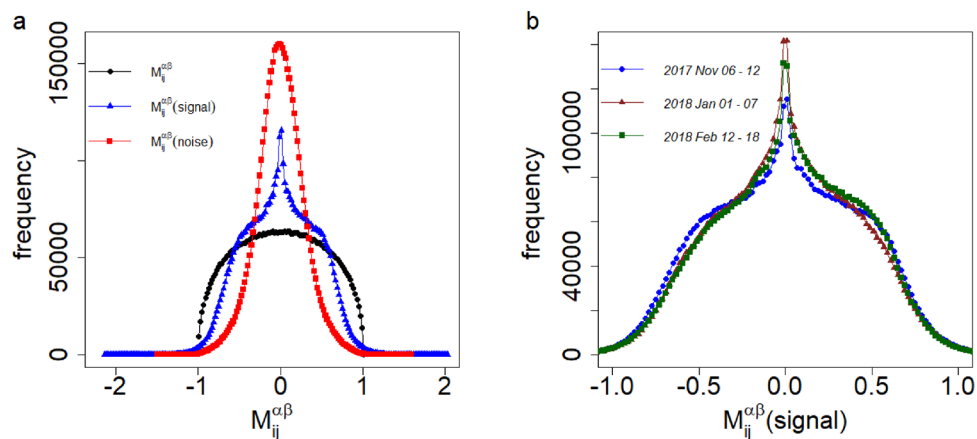


Figure 6. The decomposition of the correlation tensor in the signal component and noise component. (a) Distributions for the elements of the correlation tensor, signal component and noise component for 2017, November 06–November 12. (b) Distributions for signal components of the correlation tensors before the bubble period (2017, November 06–November 12), during the bubble period (2018, January 01–January 07) and after the bubble period (2018 February 12–February 18). The legends indicate different components of correlation tensor in (a), and different periods in (b).

component is much wider than the distribution of the elements of the noise component. Figure 6b shows the distributions of the elements of the signal component for three different weeks 2017, November 06–November 12, 2018, January 01–January 07 and 2018, February 12–February 18. This reflects the fact that the distribution for 2018, January 01–January 07 has a largest peak at zero and it is narrower than the other distributions, indicating that the dependence among the components of node vectors decreases during this time. The peakedness of each distribution can be quantified by its fourth moment, which is known as kurtosis. The different moments for the elements of the signal component of correlation tensor are tabulated in Table 1. Clearly, the peakedness and spread of the distribution during 2018, January 01–January 07 are relatively higher and thinner, respectively. As the average dependence among the components of the node vectors decreases during 2018, January 01–January 07, $\rho_1^1(t)$ has the minima during this period.

To understand why the average dependence among the components of node vectors decreases during the bubble period, 2018, January 01–January 07, we investigate the change in community structure of the regular nodes. We use well known Infomap algorithm²⁴ to detect the communities in the entire weekly directed weighted networks. We observe the evolution of the number of communities of the XRP weekly network that contains at least one regular node in Fig. 7a. It is observed that the number of such communities decreases from around 40 to around 20 during the week 2017 December 04–December 10 and the week 2017 December 18–December 24. At the same duration, we observe that the maximum number of regular nodes in a community increases from around 10 to around 50, as shown in Fig. 7b. We further delve deeper into the community structure and observe the evolution of each regular node within the communities of the weekly networks. The evolution is shown in SI Figs. S3–S6. It shows that a big community of regular nodes forms during 2017, December 18 to December 24, as shown in SI Figs. S4, S5. This big community got fragmented in subsequent weeks. Moreover, the large community of the regular nodes remains almost intact during the non-bubble period. This distinctive change in the community structure might be related to the decrease in the average dependence among the components of node vectors or the appearance of minima for the largest singular value $\rho_1^1(t)$ during the bubble period compared with non-bubble period.

Finally, using RMT^{25–28}, we show the relationship between the largest singular value and the standard deviation for the correlation tensor with normally distributed elements in Fig. 8. For the detail calculation, see the “Data and methods” section. It also shows the deviation of the largest singular values for randomized correlation tensors calculated with different time windows. It is observed that as we increase the time window to measure the randomized correlation tensor, the largest singular value ρ_1^1 approaches the theoretical value $\rho_1^1 = 2\sqrt{ND}\sigma$.

	2017, November 06–November 12	2018, January 01–January 07	2018, February 12–February 18
$\langle M_{ij}^{\alpha\beta}(\text{signal}) \rangle$	0.343 (0.006)	0.324 (0.005)	0.334 (0.005)
Standard deviation	0.419 (0.006)	0.401 (0.005)	0.409 (0.005)
Kurtosis	2.447 (0.035)	2.538 (0.032)	2.500 (0.029)

Table 1. The mean (for the absolute values of the elements), standard deviation and kurtosis of the signal components of correlation tensors for three different weeks. The values within the brackets indicate standard deviations of the quantities.

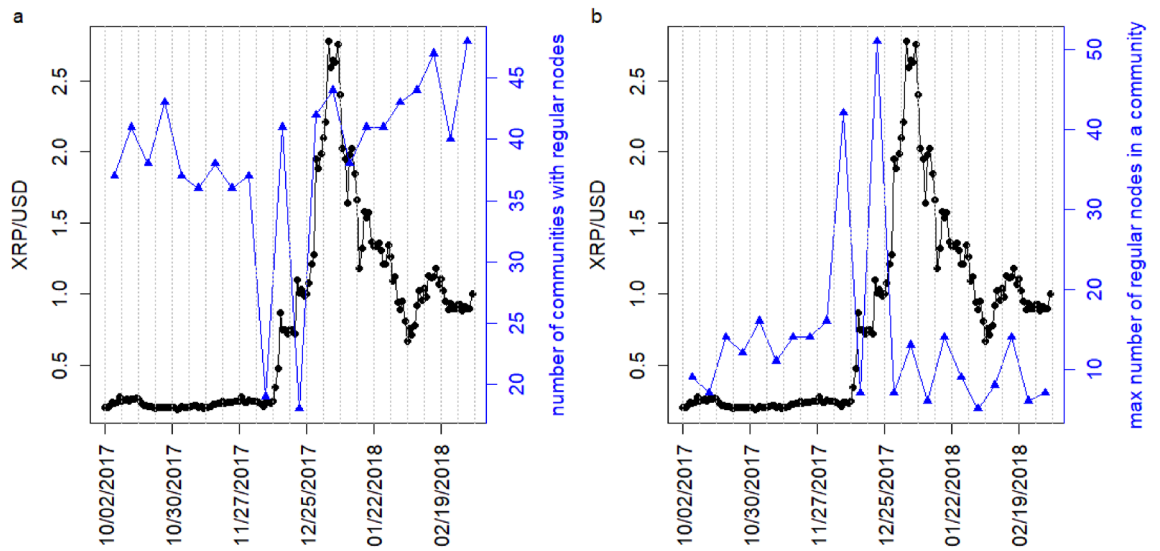


Figure 7. Evolution of regular nodes within the community structure. **(a)** Evolution of the number communities of the weekly XRP network that contains at least one regular node (blue curve). **(b)** Evolution of the maximum number of regular nodes in a community of the weekly XRP network (blue curve). The black curves in both the panels represent the daily XRP/USD price. The dotted grey vertical lines represent the weekly windows.

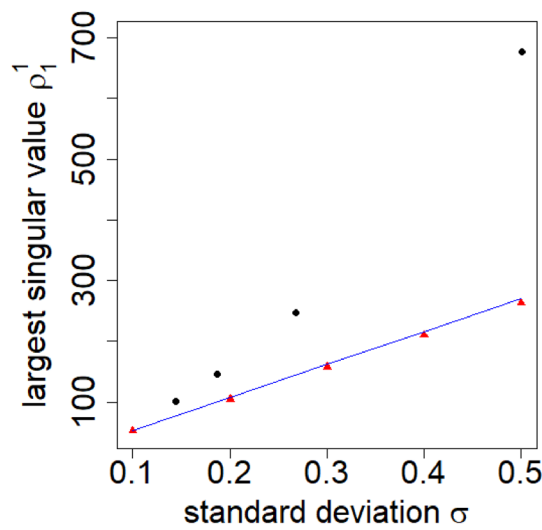


Figure 8. Plot for the largest singular value ρ_1^1 with standard deviation of the correlation tensor elements σ . Black circles represent singular values for the randomized correlation tensors with time window $(2\Delta T + 1) = 5, 15, 30$ and 50 (from right to left). Red triangles represent the largest singular values for correlation tensors, where the elements are drawn from a normal distribution with mean zero and standard deviation σ . The blue line represents $\rho_1^1 = 2\sqrt{ND}\sigma$ which is the analytical expression for the singular values as given in Eq. (11).

It reflects the fact that the noise arising from the smaller time window gradually decreases as we increase the window size.

Conclusion

In this work, we have used all the direct transactions between XRP wallets in a week to construct a weekly weighted directed network. Using the deep walk method, we have embedded weekly snapshots of the network in vector space. Deep walk encodes community information into nodal vectors using truncated random walks on the network. One can explore other methods of embedding, such as node2vec, to study other regularities of the network. From the weekly snapshots of the regular nodal vector components, we calculate the correlation tensor at different time periods. We have used a double SVD to remove redundant information from the correlation

tensor. The significance of our result is shown by comparing it with the results of a randomized counterpart. The evolution of the largest singular value ρ_1^1 shows distinctive behavior and it correlates significantly with the XRP/USD price. The decomposition of the correlation tensor into signal and noise components shows that correlation in the signal component decreases significantly during the bubble period. We explain this decrease in the correlation during the bubble period by the evolution of community structure that shows disruptive behavior during the bubble period. The disruptive behavior of community structure has also been observed in the foreign exchange market during economic downturns¹⁷.

In summary, we have developed a method of correlation tensor spectra from XRP transactions. The eigenvalue decomposition of cross correlation matrix is extensively used to analyze time series data, such as daily stock price, foreign exchange rate, etc. However interactions between the agents in these systems have not been considered. On the other hand, we construct the correlation tensor from the network structure of XRP transactions. Then the double singular value decomposition of the correlation tensor reveals a connection between the network structure and XRP price. The method also provides crucial insights into the bubble period of the XRP price. While the main focus of this study is to demonstrate the feasibility of the method, further comprehensive analysis on other bubble and non-bubble periods will be studied in the future. Overall, this method has the potential to contribute to a better understanding and detection of bubbles in financial markets. Moreover, this method is very general and can be used to analyze the transactions of other assets.

Data and methods

Data description. We collected all the direct transactions between different XRP wallets from October 2, 2017 to March 4, 2018, which were recorded as ledger data using the Ripple Transaction Protocol. We grouped these data into $T = 22$ weekly XRP networks where wallets are the nodes and a direct transaction from a source wallet to a destination wallet forms a directed link between them. The link weight between a pair of wallets is determined by the sum of XRP amounts for all transactions between them in a given week. See¹¹ for the structural properties of the XRP transaction network.

Network embedding. We embedded weighted directed weekly networks using well-known node2vec method²³ with parameters $p = q = 1$, which is a special case of the node2vec method and represents the DeepWalk method. Based on a natural language model, these embedding methods capture structural regularities in the network. Particularly, the DeepWalk method encodes the community structure in the vector representation of the nodes. It uses a truncated random walks to extract the neighborhood information of nodes by generating a sequence of nodes $S = \{V_1, V_2, V_3, \dots, V_S\}$ that is equivalent to a sentence in natural language. Furthermore, it applies SkipGram algorithm²⁹ to map each node V_j to its vector representation $\Phi(V_j) \in \mathcal{R}^D$ by maximizing the co-occurrence probability of its neighbours in the random walk.

Double singular value decomposition. To find the spectrum of the correlation tensor, we perform a double SVD in the following way:

We conduct the diagonalization of $M_{ij}^{\alpha\beta}$ in terms of (ij) -index and $(\alpha\beta)$ -index successively by the bi-unitary transformation or equivalently SVD.

The first step is

$$M_{ij}^{\alpha\beta} = \sum_{k=1}^N L_{ik} \sigma_k^{\alpha\beta} R_{kj}, \quad (2)$$

and the second step is

$$\sigma_k^{\alpha\beta} = \sum_{\gamma=1}^D \mathcal{L}^{\alpha\gamma} \rho_k^\gamma \mathcal{R}^{\gamma\beta}. \quad (3)$$

Then, altogether we have

$$M_{ij}^{\alpha\beta} = \sum_{k=1}^N \sum_{\gamma=1}^D \rho_k^\gamma (L_{ik} R_{kj}) (\mathcal{L}^{\alpha\gamma} \mathcal{R}^{\gamma\beta}). \quad (4)$$

Here ρ_k^γ is the $N \times D$ generalized singular values. Also, note that all singular values are real and positive because the correlation tensor M is real.

Reference correlation tensors. We examine the properties of the empirical correlation tensor by comparing the same quantity between the original correlation tensor and reference correlation tensors, which is analogous to random matrix theory. To get the reference correlation tensors, we have used two different techniques to obtain a reshuffled correlation tensor and a randomized correlation tensor in the following way:

Reshuffle correlation tensor. We reshuffle the components of embedding vectors $V_i^\alpha(t)$ within the time window $(2\Delta T + 1)$. Then, calculate the correlation tensor using Eq. (1) with the reshuffled embedding vector components.

Randomize correlation tensor. We assign uniform random numbers between $[-1, 1]$ to the components of embedding vectors and calculate the correlation tensor using Eq. (1).

Signal and noise components of the correlation tensor. Equation (4) can be used for dimensionality reduction to capture important relationships in the data and it can be written as

$$M_{ij}^{\alpha\beta} = M_{ij}^{\alpha\beta}(\text{signal}) + M_{ij}^{\alpha\beta}(\text{noise}), \quad (5)$$

where

$$M_{ij}^{\alpha\beta}(\text{signal}) = \rho_1^1(L_{i1}R_{1j})(\mathcal{L}^{\alpha,1}\mathcal{R}^{1,\beta}), \quad (6)$$

and

$$M_{ij}^{\alpha\beta}(\text{noise}) = \sum_{k=1}^N \sum_{\gamma=1}^d \rho_k^\gamma(L_{ik}R_{kj})(\mathcal{L}^{\alpha,\gamma}\mathcal{R}^{\gamma,\beta}) - \rho_1^1(L_{i1}R_{1j})(\mathcal{L}^{\alpha,1}\mathcal{R}^{1,\beta}). \quad (7)$$

The signal component is calculated using the singular values that lie above the largest singular values of the randomized correlation tensor. In our study, we find that only ρ_1^1 lies above the largest singular values of the randomized correlation tensor and it provides the dominant contributions to the correlation tensor.

Singular values of the correlation tensor with normally distributed elements. Let us first consider the case of a $p \times q$ random matrix R , where the elements of R are normally distributed with zero mean and standard deviation σ_R . The singular values s of such a matrix R follows the following distribution^{25,26}

$$P(s) = \frac{1}{\pi s \sigma_R^2} \sqrt{(s_{max}^2 - s^2)(s^2 - s_{min}^2)} \quad (8)$$

for $s_{min} < s < s_{max}$ and zero otherwise, where

$$s_{max} = \sqrt{2}\sigma_R \sqrt{\frac{(p+q)}{2} + \sqrt{pq}} \quad (9)$$

and

$$s_{min} = \sqrt{2}\sigma_R \sqrt{\frac{(p+q)}{2} - \sqrt{pq}} \quad (10)$$

When $p = q = N$ and $\sigma_R = \sigma$, $s_{max} = 2\sigma\sqrt{N}$. Now consider the case of the $(N \times N \times D \times D)$ random correlation tensor M_{ran} , where its elements are normally distributed with zero mean and standard deviation σ . The random correlation tensor M_{ran} contains D^2 number of $(N \times N)$ random matrix R . Analogous to Eq. (2), SVD of the random correlation tensor will give $\sigma_k^{\alpha\beta}(ran)$, where $\sigma_1^{\alpha\beta}(ran)$ is a $(D \times D)$ matrix, where its elements are distributed with mean $2\sigma\sqrt{N}$. A further SVD of $\sigma_1^{\alpha\beta}(ran)$ corresponding to Eq. (3), will give²⁷

$$\rho_1^1 = 2\sigma\sqrt{ND} + O(\sqrt{D}). \quad (11)$$

We show how the largest singular values of randomized correlation tensors deviate from the largest singular values of correlation tensors where its elements are drawn from a normal distribution with mean zero and standard deviation σ in Fig. 8.

Data availability

We collected the data from the ripple data API at <https://xrpl.org/data-api.html#payment-objects>.

Received: 28 November 2022; Accepted: 20 March 2023

Published online: 22 March 2023

References

- Wu, J., Liu, J., Zhao, Y. & Zheng, Z. Analysis of cryptocurrency transactions from a network perspective: An overview. *J. Netw. Comput. Appl.* **190**, 103139 (2021).
- Kondor, D., Pósfai, M., Csabai, I. & Vattay, G. Do the rich get richer? An empirical analysis of the bitcoin transaction network. *PLoS ONE* **9**, e86197 (2014).
- Ferretti, S. & D'Angelo, G. On the ethereum blockchain structure: A complex networks theory perspective. *Concurr. Comput. Pract. Experience* **32**, e5493 (2020).
- Tasca, P., Hayes, A. & Liu, S. The evolution of the bitcoin economy: Extracting and analyzing the network of payment relationships. *J. Risk Financ.* **19**(2), 94–126 (2018).
- Liang, J., Li, L. & Zeng, D. Evolutionary dynamics of cryptocurrency transaction networks: An empirical study. *PLoS ONE* **13**, e0202202 (2018).
- Bai, Q., Zhang, C., Xu, Y., Chen, X. & Wang, X. Poster: Evolution of ethereum: A temporal graph perspective. In *2020 IFIP Networking Conference (Networking)*, 652–654 (2020).
- Kristoufek, L. Bitcoin meets google trends and wikipedia: Quantifying the relationship between phenomena of the internet era. *Sci. Rep.* **3**, 1–7 (2013).

8. Koutmos, D. Bitcoin returns and transaction activity. *Econ. Lett.* **167**, 81–85 (2018).
9. Ciaian, P., Rajcaniova, M. & Kancs, D. The economics of bitcoin price formation. *Appl. Econ.* **48**, 1799–1815 (2016).
10. Moreno-Sanchez, P., Modi, N., Songhela, R., Kate, A. & Fahmy, S. Mind your credit: Assessing the health of the ripple credit network. In *Proceedings of the 2018 World Wide Web Conference*, 329–338 (2018).
11. Ikeda, Y. Characterization of xrp crypto-asset transactions from networks scientific approach. In *Digital Designs for Money, Markets, and Social Dilemmas*, 203–220 (Springer, 2022).
12. Aoyama, H., Fujiwara, Y., Hidaka, Y. & Ikeda, Y. Cryptoasset networks: Flows and regular players in Bitcoin and XRP. *PLoS ONE* **17**, e0273068 (2022).
13. Laloux, L., Cizeau, P., Bouchaud, J.-P. & Potters, M. Noise dressing of financial correlation matrices. *Phys. Rev. Lett.* **83**, 1467 (1999).
14. Plerou, V., Gopikrishnan, P., Rosenow, B., Amaral, L. A. N. & Stanley, H. E. Universal and nonuniversal properties of cross correlations in financial time series. *Phys. Rev. Lett.* **83**, 1471 (1999).
15. Plerou, V. *et al.* Random matrix approach to cross correlations in financial data. *Phys. Rev. E* **65**, 066126 (2002).
16. Chakraborty, A., Easwaran, S. & Sinha, S. Deviations from universality in the fluctuation behavior of a heterogeneous complex system reveal intrinsic properties of components: The case of the international currency market. *Phys. A Stat. Mech. Appl.* **509**, 599–610 (2018).
17. Chakraborty, A., Easwaran, S. & Sinha, S. Uncovering the hierarchical structure of the international forex market by using similarity metric between the fluctuation distributions of currencies. *Acta Physica Polonica A* **138** (2020).
18. Kichikawa, Y., Iyetomi, H., Aoyama, H., Fujiwara, Y. & Yoshikawa, H. Interindustry linkages of prices-analysis of Japan's deflation. *PLoS ONE* **15**, e0228026 (2020).
19. Schindler, K., Leung, H., Elger, C. E. & Lehnertz, K. Assessing seizure dynamics by analysing the correlation structure of multi-channel intracranial EEG. *Brain* **130**, 65–77 (2007).
20. Kondor, D., Csabai, I., Szüle, J., Pósfai, M. & Vattay, G. Inferring the interplay between network structure and market effects in bitcoin. *New J. Phys.* **16**, 125003 (2014).
21. Podobnik, B., Horvatic, D., Petersen, A. M. & Stanley, H. E. Cross-correlations between volume change and price change. *Proc. Natl. Acad. Sci.* **106**, 22079–22084 (2009).
22. Perozzi, B., Al-Rfou, R. & Skiena, S. Deepwalk: Online learning of social representations. In *Proceedings of the 20th ACM SIGKDD International Conference on Knowledge Discovery and Data Mining*, 701–710 (2014).
23. Grover, A. & Leskovec, J. node2vec: Scalable feature learning for networks. In *Proceedings of the 22nd ACM SIGKDD International Conference on Knowledge Discovery and Data Mining*, 855–864 (2016).
24. Rosvall, M. & Bergstrom, C. T. Maps of random walks on complex networks reveal community structure. *Proc. Natl. Acad. Sci.* **105**, 1118–1123 (2008).
25. Sengupta, A. M. & Mitra, P. P. Distributions of singular values for some random matrices. *Phys. Rev. E* **60**, 3389 (1999).
26. Rudelson, M. & Vershynin, R. Non-asymptotic theory of random matrices: extreme singular values. In *Proceedings of the International Congress of Mathematicians 2010 (ICM 2010) (In 4 Volumes) Vol. I: Plenary Lectures and Ceremonies Vols. II–IV: Invited Lectures*, 1576–1602 (World Scientific, 2010).
27. Bryc, W. & Silverstein, J. W. Singular values of large non-central random matrices. *Random Matrices Theory Appl.* **9**, 2050012 (2020).
28. Edelman, A. & Rao, N. R. Random matrix theory. *Acta Numerica* **14**, 233–297 (2005).
29. Mikolov, T., Chen, K., Corrado, G. & Dean, J. Efficient estimation of word representations in vector space. arXiv preprint [arXiv: 1301.3781](https://arxiv.org/abs/1301.3781) (2013).

Acknowledgements

We thank the members of the Kyoto Univ.- RIKEN blockchain study group for discussions. This work is partially supported by Ripple Impact Fund 2022-247584 (5855).

Author contributions

All authors conceived and designed the study. Y.I. developed the original conceptualization. T.H. formulated a double singular value decomposition. A.C. analyzed the data. All authors discussed the results and contributed to the manuscript. A.C. wrote the paper. All authors reviewed the manuscript.

Competing interests

The authors declare no competing interests.

Additional information

Supplementary Information The online version contains supplementary material available at <https://doi.org/10.1038/s41598-023-31881-5>.

Correspondence and requests for materials should be addressed to A.C.

Reprints and permissions information is available at www.nature.com/reprints.

Publisher's note Springer Nature remains neutral with regard to jurisdictional claims in published maps and institutional affiliations.



Open Access This article is licensed under a Creative Commons Attribution 4.0 International License, which permits use, sharing, adaptation, distribution and reproduction in any medium or format, as long as you give appropriate credit to the original author(s) and the source, provide a link to the Creative Commons licence, and indicate if changes were made. The images or other third party material in this article are included in the article's Creative Commons licence, unless indicated otherwise in a credit line to the material. If material is not included in the article's Creative Commons licence and your intended use is not permitted by statutory regulation or exceeds the permitted use, you will need to obtain permission directly from the copyright holder. To view a copy of this licence, visit <http://creativecommons.org/licenses/by/4.0/>.

© The Author(s) 2023